Modeling of low-pressure barium–rare-gas discharges

G. G. Lister,[1] J. J. Curry,[2] and J. E. Lawler[2]
[1]*OSRAM SYLVANIA, Inc., 71 Cherry Hill Drive, Beverly, Massachusetts 01915*
[2]*Department of Physics, University of Wisconsin, 1150 University Avenue, Madison, Wisconsin 53706*
(Received 22 December 1999)

The fundamental principles of low-pressure discharges containing a minority of barium (5–20 mtorr) in a rare gas at pressure 1–20 torr have been investigated, using a numerical model of the positive column, with a view to assessing the potential of these discharges as a light source. The principle resonance line of neutral barium is from the $6p\,^1P_1$ state and has a wavelength of 553 nm, which is close to the center of the photopic eye response curve. This green line can be augmented by radiation from barium ions to produce a ''white'' light. Published cross-section measurements suggest that the $6p\,^1P_1$ state is heavily quenched by collisions with rare-gas atoms, reducing the radiation efficiency. The measured quenching cross section is much smaller for neon than other rare gases. Spectral line broadening by these same collisions, on the other hand, enhances the escape of radiation from the discharge through the line wings. The present paper reports the results of detailed calculations of the influence of rare-gas quenching and line broadening on discharge parameters (power balance, electric field, electron temperature, and density) as a function of discharge current, rare-gas, and barium vapor pressure.

PACS number(s): 52.80.−s

I. INTRODUCTION

Barium has been proposed as a radiator in low-pressure discharge lamps [1] because it has a strong resonance radiation line at 553 nm (553.5480 nm in air), near the maximum of the eye response curve. Further, the barium ion has strong emission lines at 455, 493, 614, and 650 nm, which can augment the predominately green neutral barium radiation to produce a ''white'' light as reported by Curry *et al.* [2].

Metallic radiators currently used in low-pressure discharge lamps are mercury and sodium. Mercury has a vapor pressure of a few mtorr at room temperature and radiates principally in the ultraviolet (UV), a phosphor being required to convert UV to visible light, with a consequent reduction in efficiency in converting one high energy UV photon to a visible photon at considerably lower energy. Sodium requires a temperature of 260 °C to attain the operating vapor pressure of 3 mtorr in low-pressure sodium lamps and the principal radiation is at 589 nm, which is a yellow light suitable for outdoor applications where color rendition is not a major consideration. Barium requires an even higher temperature (600–700 °C) to attain a vapor pressure of a few mtorr and there is a considerable spread in the published data on barium vapor pressure as a function of temperature [3–7].

In common with discharges in other metal vapors, depletion of barium by radial cataphoresis plays an important role in the discharge behavior, particularly at higher discharge powers and lower vapor pressures. This effect was first observed by Druyvesteyn [8] in low-pressure sodium lamps and its importance in these lamps has been demonstrated by extensive modeling and experimental measurements [9]. Cataphoresis has also been observed in barium vapor lasers [10] and in mercury–rare-gas fluorescent lamps [11].

Another important process in barium–rare-gas discharges is the quenching of the $6p\,^1P_1$ resonance level of barium (the upper level of the 553 nm resonance transition) by rare-gas atoms. Cross sections for this process were measured by Breckenridge and Merrow [12], who found that the cross section for neon is five times lower than for argon and six times lower than xenon. The measured cross sections are sufficiently large for this process to play an important role in both the particle balance (and therefore radiation balance) and the electrical characteristics of the discharge.

The quantitative importance of the principal physical mechanisms, particularly cataphoresis and rare-gas quenching, in low-pressure barium–rare-gas discharges has been investigated by appropriately modifying the computer code GLOMAC [13], which was developed to model the positive column of mercury–rare-gas discharges. In this paper, results of calculations of the power balance, electric field, and electron temperature in these discharges are presented as a function of discharge current, rare-gas pressure, and barium vapor pressure. The model uses the best available data for the principal processes in these discharges and the uncertainties associated with this data, together with processes for which data are not currently available, are discussed in the text.

Results predict that for discharges operating at <20 W/m, conversion of electrical energy to radiated power is maximized if neon is used as the buffer gas. However, in this case, radiation is predominately green (553 nm) while discharges using argon and xenon radiate a higher fraction of input power from barium ions, and therefore a ''whiter'' light. This result qualitatively confirms results previously reported [2], using a simpler model for barium discharges containing argon as buffer gas, in which it was shown that at higher discharge currents ($\sim$1 A) the fractional power from ionic lines was comparable to or in excess of the fraction from neutral barium. The inclusion of other effects in the present paper, in particular two step ionization via intermediate metastable states, has substantially modified the quantitative conclusions drawn in that paper.

The physical processes included in the numerical model are discussed in Sec. II and the data used for the calculations is summarized in Sec. III. The results of a set of calculations

TABLE I. Energy levels for Ba included in the model.

Ba	eV
$6\ ^1S_0$	0
$5d\ ^3D_1$	1.12
$5d\ ^3D_2$	1.14
$5d\ ^3D_3$	1.19
$5d\ ^1D_2$	1.41
$6p\ ^3P_0$	1.52
$6p\ ^3P_1$	1.57
$6p\ ^3P_2$	1.68
$6p\ ^1P_1$	2.24
Ba^+	
$6\ ^2S_{3/2}$	5.21
$5\ ^2D_{3/2}$	5.82
$5\ ^2D_{5/2}$	5.92
$6\ ^2P_{1/2}$	7.73
$6\ ^2P_{3/2}$	7.94

appropriate to a discharge of internal diameter (ID) of 1 cm are discussed in Sec. V, and some conclusions from this work are discussed in Sec. VI.

II. THE PHYSICAL MODEL

The discharge is maintained by a constant electric current such that the rate of ionization exactly equals the diffusion of ions and electrons to the walls. Since electrons have a higher mobility than ions, the ambipolar radial electric field is established to ensure equal flow of electrons and ions to maintain a steady state. The electron temperature in the discharge is assumed to be sufficiently low such that only barium atoms are excited, the rare-gas atoms remaining in their ground state. The positive column is assumed to be sufficiently long for the axial field to be uniform, and hence only radial variations in the discharge parameters need be considered.

Electrons which are accelerated in the axial electric field of the positive column dissipate their energy through collisions with particles of all other species in the discharge. The inelastic electron collisions included in the present model are excitation of barium atoms from the ground state, deexcitation to the ground state (super elastic collisions), and ionization from ground and excited states. The energy expended in this process is either radiated or lost to the walls by diffusion. Elastic collisions between electrons and other species in the discharge determine the electrical conductivity and hence the electrical characteristics of the discharge. Elastic collisions between electrons and atoms and ions produce gas heating.

The excited states of barium atoms and ions considered in the model and their excitation potentials are listed in Table I. In the present model, the barium atom has two radiative states ($6p\ ^3P_1$ and $6p\ ^1P_1$) and two excited ionic states ($6p\ ^2P_{1/2}$ and $6p\ ^2P_{3/2}$) have radiative transitions to lower levels.

The following inelastic processes between excited barium atoms and ground state rare-gas atoms are also included

$$\mathrm{Ba}(6p\ ^1P_1)+X\rightarrow \mathrm{Ba}(6p\ ^3P_2)+X,$$

$$\mathrm{Ba}(6p\ ^3P_1)+X\rightarrow \mathrm{Ba}(5d\ ^1D_2)+X,$$

$$\mathrm{Ba}(5d\ ^1D_2)+X\rightarrow \mathrm{Ba}(5d\ ^3D_3)+X,$$

where X represents a ground state rare-gas atom. The energy lost by excited barium atoms in this process is assumed to be converted to gas heat.

The electron density is assumed to be sufficiently high for the electrons to follow a Maxwell-Boltzmann energy distribution, defined through the electron energy probability function (EEPF),

$$f(\varepsilon)=\frac{2}{\sqrt{\pi}(kT_e)^{3/2}}\exp(-\varepsilon/kT_e) \tag{1}$$

ε is the electron energy, T_e is the electron temperature, and $\int_0^\infty \varepsilon^{1/2} f(\varepsilon)d\varepsilon=1$.

III. THEORETICAL MODEL AND BASIC EQUATIONS

A. Ambipolar diffusion

Since the electron and ion motion in the positive column is collision dominated, the Schottky model for ambipolar diffusion is appropriate,

$$\frac{1}{r}\frac{\partial}{\partial r}\left(rD_a\frac{\partial n_e}{\partial r}\right)\approx -S_e=-n_e\sum_j Z_{ji}n_j, \tag{2}$$

where D_a is the ambipolar diffusion coefficient, n_e is the electron density, S_e is the net particle production rate per unit volume of electrons, n_j is the density of barium atoms in state j, and Z_{ji} is the ionization rate coefficient from state j,

$$Z_{ji}=\left(\frac{2}{m_e}\right)^{1/2}\int_0^\infty f(\varepsilon)q_{ji}(\varepsilon)\varepsilon\, d\varepsilon \tag{3}$$

and $q_{ji}(\varepsilon)$ is the cross section for this process. The ambipolar diffusion coefficient is

$$D_a=\frac{\mu_i D_e+\mu_e D_i}{\mu_e+\mu_i}\approx\frac{\mu_i kT_e}{e}, \tag{4}$$

where μ_e, μ_i, D_e, and D_i are electron and ion mobility and diffusion coefficients, respectively.

Boundary condition: The ion flux at the sheath edge near the wall obeys the Bohm criterion $\Gamma_i(R)=n_e v_s$ where $v_s=(kT_e/M)^{1/2}$ and M is the mass of the barium ion. Equating this flux to the ambipolar flux gives

$$-D_a\frac{dn_e}{dr}=n_e v_s. \tag{5}$$

B. Neutral particle diffusion and radiation transport

1. Ground state and metastable diffusion

The diffusion equations for ground state and metastable barium atoms in electronic state j can been represented in the form [14]

$$\frac{1}{r}\frac{\partial}{\partial r}\left[rD_jN\frac{\partial}{\partial r}\left(\frac{n_j}{N}\right)\right]+n_e\sum_k\ (Z_{kj}n_k-Z_{jk}n_j)$$

$$+n_X\sum_k\ (C_{kj}^{\mathrm{Ba}-X}n_k-C_{jk}^{\mathrm{Ba}-X}n_j)=0, \tag{6}$$

where N is the total gas density and D_j is the diffusion coefficient for atoms in state j, Z_{jk} is the electron-impact rate coefficient for the transition $j\rightarrow k$ [cf. Eq. (3), substituting $q_{jk}(\varepsilon)$, the cross section for this process], $C_{jk}^{\mathrm{Ba}-X}$ is the reaction rate coefficient for the process

$$\mathrm{Ba}_j+X\rightarrow\mathrm{Ba}_k+X,$$

where X represents a ground state atom of the buffer gas, density n_X. Metastable atoms and ions diffuse outwards to the walls, while ground state atoms diffuse inwards at a much slower rate than ions, leading to barium depletion in the center of the discharge (cataphoresis).

Boundary conditions: For metastable state (cf. [15], p. 14) the particle flux to the wall is

$$\Gamma_j=-D_jN\frac{\partial}{\partial r}\left(\frac{n_j}{N}\right)=\frac{1}{4}n_jv_a, \tag{7}$$

where $v_a=(8kT_g/\pi M)^{1/2}$ is the particle thermal velocity.

2. Radiation transport

A barium atom in radiative state j will decay much faster than the time scale for diffusion to the wall and these states satisfy a set of rate equations

$$n_e\sum_k\ (Z_{kj}n_k-Z_{jk}n_j)+n_X\sum_k\ (C_{kj}^{\mathrm{Ba}-X}n_k-C_{jk}^{\mathrm{Ba}-X}n_j)$$

$$+\sum_k\ (\beta_{jk}n_j-\beta_{kj}n_k)=0, \tag{8}$$

where β_{jk} s^{-1} is the fundamental mode trapped decay rate for the transition $j\rightarrow k$ [16]. Lawler and Curry [17] developed an analytic formula for β_{jk} for resonance lines as a function of the ground state density n_0, gas temperature T_g, and the discharge radius R, based on extensive Monte Carlo calculations, for the case of uniform ground state density and negligible isotopic and hyperfine structure. This formula includes the effect of partial frequency redistribution in a realistic fashion. It has also been modified to include the influence of foreign gas broadening [18] and nonuniform distributions of ground state atoms, such as are produced by cataphoresis [19]. For details of the formula used in this work, the reader is referred to Refs. [18] and [19].

We ignore the effect of hyperfine and isotopic structure on the fundamental mode trapped decay, as it is expected to be small. Approximately 72% of naturally occurring Ba is ^{138}Ba with no hyperfine structure. Considering the resonance line at 553 nm, only approximately 3% of the total line strength is shifted by more than 305 MHz [20]. The half-width at $1/e$ max of the Doppler line shape, in comparison, is approximately 600 MHz at an operating temperature of 650 °C.

C. Electron energy balance

The equation for the energy balance per unit length in the discharge is (see the Appendix)

$$W_{\mathrm{tot}}=I_eE_z$$

$$=2\pi\int_0^R r\,dr[H_{\mathrm{inel}}(r)+H_{\mathrm{el}}(r)]+2\pi R(\varepsilon_w+V_w)j_r^+(R), \tag{9}$$

where W_{tot} is the total electrical power (per unit length) in the positive column of the discharge $I_e=2\pi\int_0^R rj_z^-(r)dr$ is the total electron discharge current,

$$j_z^-=\sigma_eE_z, \tag{10}$$

$\sigma_e=en_e\mu_e$ is the electrical conductivity, $H_{\mathrm{inel}}(r)$ and $H_{\mathrm{el}}(r)$ are the net collisional rates per unit volume of electron energy loss due to inelastic and elastic collisions, respectively, ε_w is the average energy of electron reaching the wall (assumed to be $3kT_e/2$), V_w is the potential drop in the sheath, and $j_r^+(R)=e\Gamma^+(R)$ is the ion current density to the wall.

For a Maxwellian EEPF (1), the electron mobility μ_e is

$$\mu_e=\frac{e}{3NkT_e}\left(\frac{2}{m_e}\right)^{1/2}\int_0^\infty\frac{\varepsilon}{q_t(\varepsilon)}f(\varepsilon)d\varepsilon, \tag{11}$$

where $q_t(\varepsilon)$ is the total electron transport cross section

$$q_t(\varepsilon)=q_{\mathrm{em}}(\varepsilon)+q_{\mathrm{inel}}(\varepsilon)+\frac{n_e}{N}\frac{q_e(\varepsilon)}{\gamma_E}. \tag{12}$$

$q_{em}(\varepsilon)$ is the electron momentum transfer cross section, $q_{\mathrm{inel}}(\varepsilon)$ is the total inelastic cross section, $q_e(\varepsilon)$ is the electron-ion Coulomb cross section, given in MKS units by

$$q_e(\varepsilon)=\frac{\pi}{\varepsilon^2}\left(\frac{e^2}{4\pi\varepsilon_0}\right)^2\ln\Lambda,$$

$$\ln\Lambda=-\frac{1}{2}\ln\left(\frac{n_ee^6}{9(4\pi)^2(\varepsilon_0kT_e)^3}\right), \tag{13}$$

$\gamma_E=0.582$ for a singly ionized gas [21], and

$$H_{\mathrm{inel}}(r)=n_e\sum_{j,k}\ \varepsilon_{jk}Z_{jk}n_j \tag{14}$$

where ε_{jk} is the difference in energies between levels k and j and

$$H_{\mathrm{el}}(r)=\left(\frac{2}{m_e}\right)^{1/2}Nn_e\int_0^\infty\frac{2m_e}{M}[q_{\mathrm{em}}(\varepsilon)+q_{\mathrm{inel}}(\varepsilon)]$$

$$\times\left(\varepsilon-\frac{3kT_g}{2}\right)\varepsilon f(\varepsilon)d\varepsilon. \tag{15}$$

Note that $H_{\mathrm{el}}(r)$ includes the contributions from all electron collision processes with the exception of electron–electron Coulomb interactions, which have no direct role in the electron energy balance ([22], p. 40), although they may contribute indirectly to energy dissipation in the electric field by helping to maintain the Maxwellian electron energy distribution function.

For the Maxwell-Boltznmann probability function [cf. Appendix (Eq. A10)],

$$V_w = \frac{kT_e}{2e} \ln\left(\frac{M}{2\pi m_e}\right). \tag{16}$$

For discharges in Ba, $V_w \approx 4.8\varepsilon_e$ V. The total flux of ions per unit length to the wall is equal to the electron flux, given by Eq. (5).

Detailed power balance: The detailed power balance in the positive column, in analogy to Eq. (9), is

$$W_{\text{tot}} = W_{\text{inel}} + W_{\text{el}} + W_{\text{sheath}}, \tag{17}$$

where the three terms on the RHS of (17) represent three terms on the RHS of (9). The total power per unit length dissipated in inelastic processes may be further partitioned

$$W_{\text{inel}} = W_{\text{rad}} + W_D + W_q, \tag{18}$$

where W_{rad}, W_D, and W_q represent the power per unit length dissipated by radiation, diffusion of ions and metastable atoms to the wall and quenching by rare-gas atoms, respectively.

The total power per unit length from the radiative transition $k \rightarrow j$ reaching the walls [cf. Eq. (8)] is

$$W_{\text{rad}}(\lambda_{kj}) = 2\pi\varepsilon_{jk}\beta_{jk}\int_0^R n_k(r)\, r\, dr \tag{19}$$

and

$$W_{\text{rad}} = \sum_{j,k} W_{\text{rad}}(\lambda_{kj}). \tag{20}$$

The total diffusion losses of ions and metastable atoms are obtained from Eqs. (5) and (7),

$$W_D = 2\pi R\left[\sum_j \varepsilon_j D_j N \frac{d}{dr}\left(\frac{n_j}{N}\right)\bigg|_{r=R} + \varepsilon_i D_a \left.\frac{dn_e}{dr}\right|_{r=R}\right]. \tag{21}$$

It is often convenient to combine the diffusion and sheath losses into a single term representing wall losses, $W_{\text{wall}} = W_{\text{sheath}} + W_D$. The power per unit length dissipated due to rare-gas quenching is $W_q = 2\pi\int_0^R r\, dr\, H_q(r)$, where

$$H_q(r) = n_X \sum_{j,k} \varepsilon_{jk} C_{jk}^{\text{Ba}-X} n_j. \tag{22}$$

D. Gas heating

The heat conduction equation, to compute gas temperature profiles, is

$$\frac{1}{r}\frac{d}{dr}\left(\kappa_g(T_g) r \frac{dT_g}{dr}\right) + H_{\text{el}}(r) + H_q(r) = 0, \tag{23}$$

where κ_g is the thermal conductivity of the gas. The local barium density is computed from (6), in order to account for cataphoresis. Rare-gas densities are obtained from Charles law

TABLE II. (a) Cross section at 693 K (units 10^{-20} m^2). (b) Rate coefficients at 880 K (units 10^{-18} m^3 s^{-1}) for barium atom collisions with rare-gas atoms.

Rare gas	$6p\,^1P_1 \rightarrow 6p\,^3P_2$ (a)	$6p\,^3P_1 \rightarrow 5d\,^1D_2$ (b)	$5d\,^1D_2 \rightarrow 5d\,^3D_3$ (b)
Ne	0.43 ± 0.16	40 ± 3	3.51 ± 0.18
Ar	2.5 ± 0.6	43 ± 2	0.29 ± 0.04
Kr	3.9 ± 2.0	22.9 ± 1.4	0.10 ± 0.04
Xe	3.1 ± 1.0	5.9 ± 0.3	3.28 ± 0.20

$$2\pi p_g \int_0^R \frac{r\, dr}{kT_g(r)} = N_T, \tag{24}$$

$$p_g = N(r) k T_g(r), \tag{25}$$

where p_g is the (constant) partial gas pressure and N_T is the total number of atoms per unit length. The wall temperature T_w is an input parameter, typically the estimated value of the cold spot temperature.

IV. DATA

A. Electron impact cross sections

Cross sections for excitation of the $6p\,^1P_1$ and ionization from the ground state have been measured by Chen and Gallagher [23] and Dettmann and Karstensen [24], respectively. Excitation of all other neutral barium excited states in Table I have been computed by Fursa and Bray [25] using close coupling calculations. The good agreement obtained between the calculated and experimentally measured values for the excitation cross section of $6p\,^1P_1$ from the ground state lends confidence in the accuracy of these calculations.

The only cross section for transitions between excited states available in the literature is that of $6p\,^1P_1$ from the state $5d\,^1D_2$, for which measured and calculated values are presented in Johnson *et al.* [26]. Cross sections for ionization from excited states j are computed from the formula by Vriens and Smeets [27]

$$q_{ji}(\varepsilon) = \frac{\pi}{\varepsilon + 3.25\varepsilon_{ji}}\left(\frac{e^2}{4\pi\varepsilon_0}\right)^2\left(\frac{5}{3\varepsilon_{ji}} - \frac{1}{\varepsilon} - \frac{2}{3}\frac{\varepsilon_{ji}}{\varepsilon^2}\right), \tag{26}$$

where ε_{ji} is the ionization potential (in joules) from state j.

Excitation to the ionic levels $6p\,^2P_{1/2,3/2}$ from the ionic ground state have been measured by Crandall *et al.* [28]. These states are assumed to radiate instantaneously, either to the ionic ground state or $5\,^2D_{3/2,5/2}$ levels (cf. Sec. IV C). Ions in state $5\,^2D_{3/2,5/2}$ populated by the above radiative transitions are assumed to return instantly to the ionic ground state due to collisions of the second kind, hence their population density is not computed in the model.

B. Diffusion and collisional processes in rare gases

The most important atomic process involving barium and rare-gas atoms reported in the literature [12] is the quenching of the $6p\,^1P_1$ state of barium to the $6p\,^3P_2$ state, for which cross sections are listed in column 1 of Table II. Rate coef-

ficients for quenching of other radiative states have been measured by Brust and Gallagher [29] and the most important of these are listed in Table II.

Diffusion coefficients for Ba($5d\,^3D_2$) state have been measured by Walker *et al.* [30]. The diffusion coefficients D_0 at 273 K and 1 atm pressure are $D_0 = 2.01 \times 10^{-5}\,m^2\,s^{-1}$ (Ne), $1.43 \times 10^{-5}\,m^2\,s^{-1}$ (Ar), and $8.40 \times 10^{-6}\,m^2\,s^{-1}$ (Xe). These values are assumed also for diffusion of the ground state of Ba and all nonradiative excited states.

The mobility of barium ions in argon at 1 atmosphere pressure and 273 K is quoted by Viehland and Mason [31] as $\mu_{i0} = 1.79 \times 10^{-4}\,m^2\,V\,s^{-1}$. No values are given for neon or xenon. However, values for the ion mobilities for cesium in all rare gases are given by McDaniel and Mason [32] and the values in helium and argon are within 15% of the values for barium. The barium ion mobilities in neon and xenon are therefore set to the cesium values—$6.0 \times 10^{-4}\,m^2\,V^{-1}\,s^{-1}$ (Ne) and $9.1 \times 10^{-5}\,m^2\,V^{-1}\,s^{-1}$ (Xe). The mobility in the discharge is computed using the factor $\mu_i = \mu_{i0} N_a / N$, where N_a is the gas density at 1 atmosphere and 273 K and N is the gas density in the discharge.

C. Radiation transport parameters

The Einstein coefficients for the spectral lines included in the program are from Fuhr and Wiese [33] and are listed below

Neutral lines	λ_0 nm	$A_{jk}\ s^{-1}$
$6p\,^3P_1 \rightarrow 6s\,^1S_0$	791.2	2.98×10^5
$6p\,^1P_1 \rightarrow 6s\,^1S_0$	553.6	1.19×10^8
$6p\,^1P_1 \rightarrow 5d\,^3D_2$	1129.9	1.20×10^5
$6p\,^1P_1 \rightarrow 5d\,^1D_2$	1500.2	2.8×10^5
Ion lines		
$6s\,^2P_{1/2} \rightarrow 6s\,^2S_{1/2}$	493.4	9.55×10^7
$6s\,^2P_{3/2} \rightarrow 6s\,^2S_{1/2}$	455.4	1.17×10^8
$6s\,^2P_{1/2} \rightarrow 5\,^2D_{3/2}$	649.7	3.32×10^7
$6s\,^2P_{3/2} \rightarrow 5\,^2D_{5/2}$	614.2	3.70×10^7

Broadening of the 553 nm line due to collisions with argon and helium atoms has been measured by Ehrlacher and Huennekens [34]. The van der Waals coefficient [18] for argon was found to be $B = (3.6/2\pi) \times 10^{-15}\,m^3\,s^{-1}$, and for helium was found to be $B = (3.9/2\pi) \times 10^{-15}\,m^3\,s^{-1}$. Due to the fact that the coefficient varies by only 10% between argon and helium, we have assumed the argon value for all gases. All ionic lines are assumed to be optically thin.

V. RESULTS AND DISCUSSION

A number of calculations have been performed to demonstrate the influence of discharge current, rare-gas type and pressure, and barium vapor pressure on the performance of low-pressure barium discharges. All calculations have assumed an inner diameter of 10 mm. Calculations have been performed for discharges in Ne, Ar, and Xe, with rare-gas pressures of 1 to 15 torr at room temperature, barium vapor pressure of 5–20 mtorr and discharge currents of 100 mA to 1 A. Results are presented as a function of barium vapor pressure rather than cold spot temperature, in view of the broad spread of barium vapor pressure data in the literature. Our best estimates indicate that the range considered corresponds to a cold spot temperature ~600–700 °C. Not all values in this parameter range are accessible to the current version of the code, due to lack of convergence in cases of strong cataphoresis. This is particularly true in the case of neon, which has a much higher ion mobility (and therefore ambipolar diffusion coefficient) than argon and xenon. The convergence problems arise because there are insufficient barium atoms at the center of the discharge to provide the necessary particle balance at any electron temperature. In these cases, we would expect rare-gas excitation to become important, but this effect is not included in the current model.

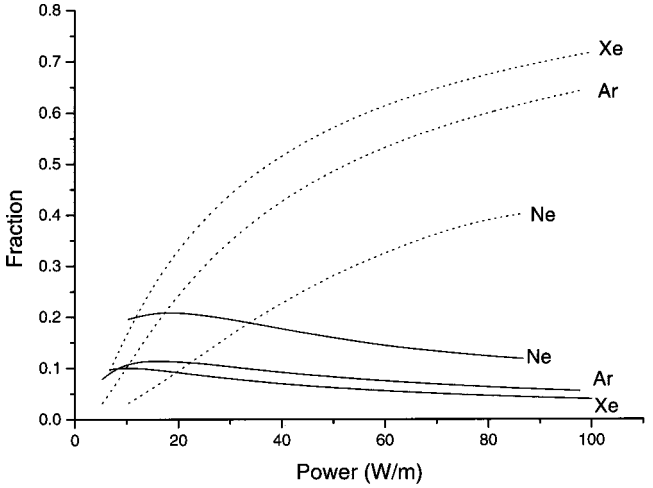

FIG. 1. Fraction of total input power converted to visible radiation as a function of total power per unit length in the positive column for a discharge containing 12 mtorr Ba and a density of rare gas corresponding to 5 torr at 298 K, ID = 10 mm. Full lines, neutral barium radiation. Dotted lines, Ba ionic radiation.

Figure 1 shows the fraction of power converted to visible radiation, as a fraction of the total input power per unit length to the positive column in a discharge containing 5 torr of rare gas at 298 K with a barium vapor pressure of 12 mtorr. The contributions from the neutral 553 nm line and the barium ionic lines are plotted separately. Due to the reduced quenching of the $6\,^1P_1$ state by neon atoms compared to argon and xenon, the green 553 nm line is predicted to dominate the spectrum for input powers less than ~35 W/m. In discharges in argon and xenon, however, the power dissipated by ionic radiation is calculated to be equal to or greater than the contribution from the 553 nm line neutral barium radiation for almost the entire power range considered.

The influence of buffer gas pressure for the discharge considered above, operating at 400 mA, is illustrated in Figs. 2 and 3. Figure 2 shows the influence of quenching of the Ba resonance level by the rare-gas atoms, resulting in a monotonic decrease in the fraction of power converted to 553 nm radiation with increasing rare-gas pressure. However, this is compensated by an *increase* in the fraction of power converted to radiation from the barium ionic lines. Figure 3 illustrates that for constant discharge current; the total radiation from the discharge increases montonically as rare-gas pressure increases (as does total discharge power) due to the

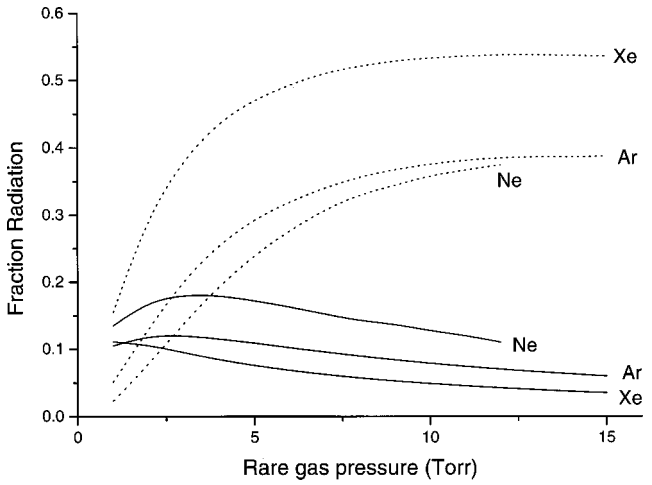

FIG. 2. Fraction of total input power converted to visible radiation as a function of rare-gas pressure for the conditions of Fig. 1, discharge current $I=400$ mA.

large decrease in wall losses at higher pressures. The increase in losses due to quenching for discharges in argon compared to neon is also graphically illustrated.

The influence of barium vapor pressure on the radiation output of the discharge is illustrated in Fig. 4. The fraction of power contained in the ionic lines decreases montonically

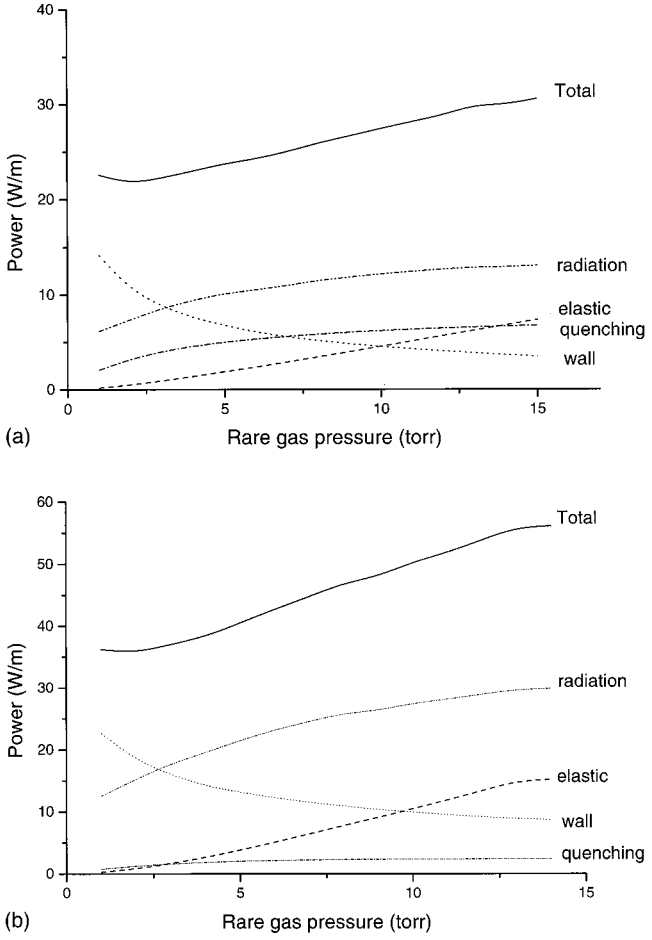

FIG. 3. Detailed power balance as a function of rare-gas pressure for the discharge for conditions of Fig. 1, $I=400$ mA. (a) Argon; (b) neon.

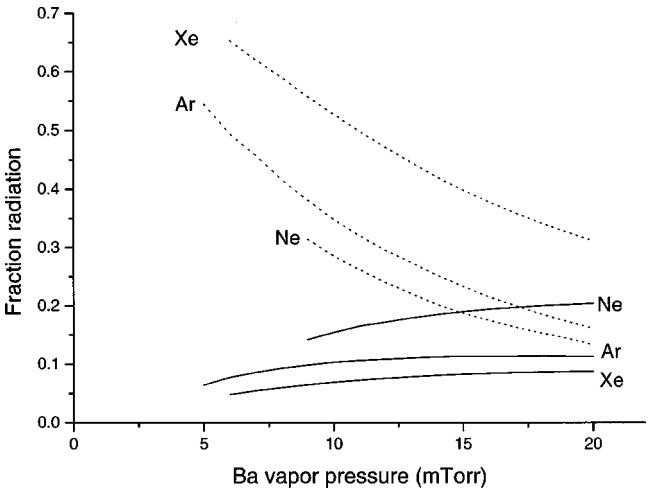

FIG. 4. Fraction of total input power converted to visible radiation as a function of Ba vapor pressure for the conditions of Fig. 1, discharge current $I=400$ mA.

with increasing vapor pressure. The fraction radiated at 553 nm saturates at sufficiently high vapor pressures, although the value at which this occurs is higher for neon than argon or xenon.

An interesting feature of Ba–rare-gas discharges is that, in common with low-pressure sodium discharges [9], the calculations predict a positive characteristic for the maintenance (axial) electric field as a function of discharge current for high currents, as illustrated in Fig. 5. In sodium discharges, this has been attributed to cataphoresis, and in barium discharges the increased quenching of the radiative states as the current increases is an additional power loss which further raises the electric field. An interesting feature in Fig. 5 is that the electric field in xenon is higher than that in argon, which is contrary to the situation observed in mercury- and sodium-rare–gas discharges. The reason for this behavior appears to be due to the existence of the ionic spectral lines in barium. The electron density is higher in discharges in xenon and argon, resulting in more power being dissipated in radiation from ionic lines, leading to a higher electric field.

Finally, it is interesting to examine the electron temperature in these discharges as a function of discharge current,

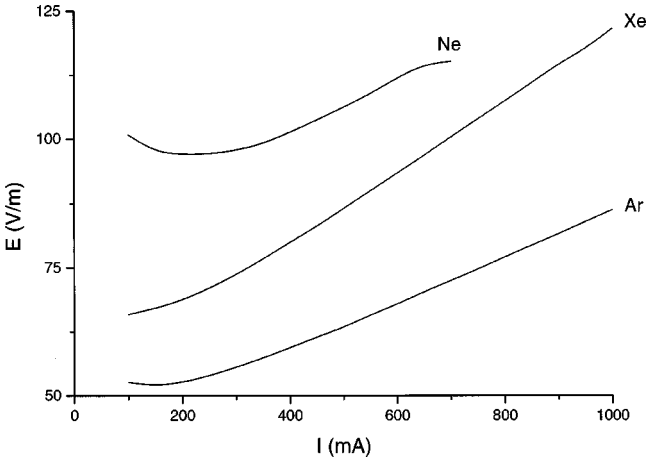

FIG. 5. Electric field E as a function of discharge current I for the conditions of Fig. 1.

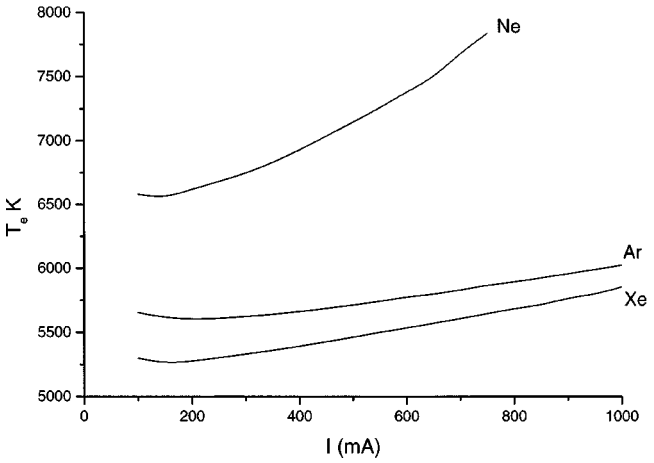

FIG. 6. Electron temperature T_e as a function of discharge current I for the conditions of Fig. 1.

which is illustrated in Fig. 6. As expected, electron temperatures are considerably lower than in comparable discharges in Hg, due to the lower ionization potential of Ba. Electron temperatures in discharges containing neon are somewhat higher than in argon and xenon, due to the higher mobility of barium ions in neon and the consequent increase in the ambipolar diffusion coefficient.

VI. CONCLUSIONS

The results of calculations described in this paper have been obtained using the best available data for the important physical processes in barium–rare-gas discharges for lighting. Calculations indicate that there is a wide range of operating parameters for which a ''white'' light source might be obtained, although the practical limitations of operating lamps under these conditions have yet to be investigated. There remains some uncertainty regarding the quenching rate for the principal resonance state in neutral barium and the broadening of this resonance line by foreign gases. Using experimentally measured values for the quenching cross sections, the calculations predict that barium discharges in neon would have higher efficacy at the same input power than discharges in either argon or xenon. However, the highest efficacy is found for lower input power, due to the increased power radiated in the green 553 nm line, and this would be less favorable for the production of ''white'' light. A further uncertainty is the knowledge of the cold spot temperature needed to attain the required barium vapor pressures.

On the basis of the reported calculations, the following conclusions may be drawn.

The green 553 nm line is predicted to dominate the ionic lines for discharges in neon for input powers ~35 W/m. In discharges in argon and xenon, however, the power dissipated by ionic radiation is calculated to be equal to or greater than the neutral barium radiation for almost the entire power range considered.

For discharges in xenon, argon, and neon, the contributions from ionic and neutral barium lines are equivalent for buffer gas pressures of about 1, 2, and 3 torr, respectively. At higher pressures, the fractional contribution from ionic lines saturates and that from the neutral barium monotonically decreases.

For discharges in argon and xenon, the fractional contribution from neutral lines appears to saturate for barium vapor pressures above about 10 mtorr. Discharges in neon do not appear to saturate until about 20 mtorr, with a predominantly green emission. The fractional ionic radiation decreases with increasing barium vapor pressure.

For the range of parameters considered, all discharges exhibit a positive $V-I$ characteristic.

The most important processes not included in the present model are the excitations between excited states by electron impact, for which there are no cross sections available in the literature. The model does not include the effects of rare-gas excitation, which may be important at higher discharge powers, where cataphoresis dominates. However, the model also suggests that in this parameter range, light output is significantly reduced.

ACKNOWLEDGMENTS

One of us (G.G.L.) is grateful for valuable discussions with Dr. P. Moskowitz and Dr. F. Palmer of OSI, and to Dr. D. Fursa of Flinders University, South Australia, for supplying tabulated data for his calculated cross sections. The research is supported in part by NSF Grant No. ECS 97-10234.

APPENDIX: THE ENERGY BALANCE EQUATION

In a collision dominated positive column, the electron drift velocity is usually much smaller than the random velocity, and therefore the electron velocity distribution function $f_e(\vec{v},\vec{r})$, where $\vec{v}$ is the velocity vector and $\vec{r}$ is the position vector, is only weakly dependent on the direction of the velocity $\vec{v}$. In this case $f_e(\vec{v},r)$ may be approximated by the sum of the first four terms of the spherical function series expansion [35],

$$f_e(\vec{v},r)=f_0(\varepsilon,r)+\frac{\vec{v}}{v}\cdot\vec{f}_1(\varepsilon,r) \tag{A1}$$

where $\varepsilon=m_e v^2/2$ is the electron energy. For the case of a steady state axially uniform cylindrical positive column, the zeroth-order expansion of the Boltzmann equation is

$$\frac{v}{3r}\frac{\partial}{\partial r}(rf_{1r})-\frac{1}{3v}\frac{\partial}{\partial\varepsilon}\{v^2(E_z f_{1z}+E_r f_{1r})\}=C(f_0), \tag{A2}$$

where $C(f_0)$ represents the rate of change of the function f_0 due to electron collisions. The spatially dependent equation of the electron energy balance per unit volume follows from Eq. (A2) applying the operator $e\int_0^\infty \varepsilon\Delta(\varepsilon)d\varepsilon$,

$$\frac{1}{r}\frac{d}{dr}(rQ_r)-E_z j_z^- - E_r j_r^- = -H, \tag{A3}$$

where $Q_r=e\langle v\varepsilon\rangle_r$ is the radial component of the electron energy flux density and [cf. Eq. (9)]

$$H(r)=-\int_0^\infty \varepsilon\Delta(\varepsilon)C[f_0(\varepsilon,r)]d\varepsilon=H_{\mathrm{inel}}(r)+H_{\mathrm{el}}(r). \tag{A4}$$

The equation for the energy balance per unit length in the discharge can be obtained from Eq. (A4) by integrating over $2\pi r\,dr$ to the tube radius R,

$$I_e E_z = 2\pi R Q_r(R) + 2\pi \int_0^R r\,dr\{H(r) + E(r) j_r^+(r)\}, \tag{A5}$$

where $I_e = 2\pi \int_0^R r j_z^-(r) dr$ is the total electron discharge current, $j_r^+ = -j_r^-$ is the radial ion current and $Q_r(R) \approx \varepsilon_w j_r^+(R)$ is the electron energy flux density to the wall, and ε_w is the average energy of electron reaching the wall. Since the radial field has a very sharp maximum in the sheath near the wall, the second term on the RHS of (A5) may be approximated by

$$\int_0^R r\,dr\,E_r(r) j_r^+(r) \approx R j_j^+(R) \int_0^R dr\,E_r(r) = R j_r^+(R) V_w, \tag{A6}$$

where V_w is the potential drop in the sheath. Finally, Eq. (A5) may be written

$$I_e E_z = 2\pi \int_0^R r\,dr\,H(r) + 2\pi R(\varepsilon_w + V_w) j_r^+(R). \tag{A7}$$

The equation for the sheath potential drop V_w is obtained, by equating the electron random velocity to the wall and ion sound velocity $v_{\rm th}$ at the plasma-sheath boundary. This gives

$$\frac{1}{4}\left(\frac{2e}{m_e}\right)^{1/2} \int_{V_w}^{\infty} (\varepsilon - V_w) f(\varepsilon, r) d\varepsilon = v_s = \left(\frac{kT_{\rm sc}}{M_s}\right)^{1/2}, \tag{A8}$$

where $T_{\rm sc}$ is the ''screening temperature'' [36]

$$kT_{\rm sc} = 2\left\{ \int_0^{\infty} \varepsilon^{-1/2} f(\varepsilon) d\varepsilon \right\}^{-1}. \tag{A9}$$

For the Maxwell-Boltznmann distribution, $T_{\rm sc} = T_e$ and

$$V_w = \frac{kT_e}{2e} \ln\left(\frac{M}{2\pi m_e}\right). \tag{A10}$$

[1] J. E. Lawler, H. M. Anderson, and J. J. Curry, in *Proceedings of the 8th International Symposium on the Science and Technology of Light Sources*, edited by Gerhard Babucke (INP, Greifswald, 1998), pp. 138, 139.

[2] J. J. Curry, H. M. Anderson, J. MacDonagh, J. E. Lawler, and G. G. Lister, J. Appl. Phys. **87**, 2058 (2000).

[3] *Smithells Metals Reference Book*, 7th ed., edited by E. A. Brandes and G. B. Brook (Butterworth-Heinemann, London, 1992).

[4] M. W. Chase, *NIST-JANAF Thermochemical Tables*, 4th ed., edited by M. W. Chase (American Chemical Society, Washington, DC, 1998).

[5] R. Hultgren *et al.*, *Selected Values of Thermodynamic Properties of the Elements* (American Society of Metals, Metals Park, OH, 1973).

[6] K. T. Jacob and Y. Waseda, J. Less-Common Met. **139**, 249 (1988).

[7] *The Characterization of High Temperature Vapors*, edited by J. L. Margrave (Wiley, New York, 1967).

[8] M. J. Druvvesteyn, Physica (Amsterdam) **1**, 14 (1933).

[9] H. van Tongeren, Philips Res. Rep., Suppl. **3**, 1 (1975).

[10] R. P. Mildren, D. J. W. Brown, and J. A. Piper, J. Appl. Phys. **82**, 2039 (1997).

[11] C. Kenty, J. Appl. Phys. **38**, 4517 (1967).

[12] W. H. Breckenridge and C. N. Merrow, J. Chem. Phys. **88**, 2329 (1988).

[13] G. G. Lister and S. E. Coe, Comput. Phys. Commun. **75**, 160 (1993).

[14] S. Chapman and T. G. Cowling, *The Mathematical Theory of Non-Uniform Gases*, 3rd ed. (Cambridge University Press, Cambridge, 1970).

[15] S. Dushman, *Scientific Foundations of Vacuum Technique*, 2nd ed. (Wiley, New York, 1949).

[16] A. F. Molisch and B. P. Oehry, *Radiation Trapping in Atomic Vapors* (Clarendon, Oxford, 1998).

[17] J. E. Lawler and J. J. Curry, J. Phys. D: Appl. Phys. **31**, 3225 (1998).

[18] J. E. Lawler, J. J. Curry, and G. G. Lister, J. Phys. D: Appl. Phys. **33**, 252 (2000).

[19] J. J. Curry, J. E. Lawler, and G. G. Lister, J. Appl. Phys. **86**, 731 (1999).

[20] P. G. Pappas, M. M. Burns, D. D. Hinshelwood, and M. S. Feld, Phys. Rev. A **21**, 1955 (1980).

[21] L. Spitzer and R. Härm, Phys. Rev. **89**, 977 (1953).

[22] Y. P. Raizer, *Gas Discharge Physics* (Springer-Verlag, Berlin, 1987).

[23] S. T. Chen and A. Gallagher, Phys. Rev. A **14**, 593 (1976).

[24] J-M. Dettmann and F. Karstensen, J. Phys. B **15**, 287 (1982).

[25] D. V. Fursa and I. Bray, Phys. Rev. A **59**, 282 (1999).

[26] P. V. Johnson, B. Eves, P. W. Zetner, D. Fursa, and I. Bray, Phys. Rev. A **59**, 439 (1999).

[27] L. Vriens and A. H. M. Smeets, Phys. Rev. A **22**, 940 (1980).

[28] D. H. Crandall, P. O. Taylor, and G. H. Dunn, Phys. Rev. A **10**, 141 (1974).

[29] J. Brust and A. C. Gallagher, Phys. Rev. A **52**, 2120 (1995).

[30] T. G. Walker, K. D. Bonin, and W. Happer, J. Chem. Phys. **87**, 660 (1987).

[31] L. A. Vriedland and E. A. Mason, At. Data Nucl. Data Tables **60**, 37 (1995).

[32] E. W. McDaniel and E. A. Mason, *The Mobility and Diffusion of Ions in Gases* (Wiley, New York, 1976).

[33] J. F. Fuhr and W. Wiese, *CRC Handbook of Chemistry and Physics*, 79th ed. (CRC Press, Boca Raton, 1998), p. 94.

[34] E. Ehrlacher and J. Huennekens J, Phys. Rev. A **47**, 3097 (1993).

[35] B. I. Davydov, Zh. Eksp. Teor. Fiz. **7**, 1064 (1937).

[36] V. A. Godyak, R. B. Piejak, and B. M. Alexandrovich, J. Appl. Phys. **73**, 3657 (1993).